and immediately processed by HPLC, the definitive method for separating and quantifying plant pigments (*101–104*) including accessory carotenoids (*105*). Chlorophyll a concentrations from all water samples were also determined fluorometrically (*106*). Nutrient and pigment concentrations are given micromoles per liter and nanomoles per liter, respectively. Here 19′-hexanoyloxyfucoxanthin (Fig. 3I) is a diagnostic tag for *Phaeocystis* spp., which dominated the near-ice phytoplankton, and fucoxanthin (Fig. 3J) is a tag for diatoms that were found further out in the MIZ.

111. B. B. Prézelin, R. R. Bidigare, H. A. Matlick, M. Putt, B. Ver Hoven, *Mar. Biol.* **96**, 563 (1987).
112. B. B. Prézelin and H. E. Glover, *J. Plankton Res.* **13** (suppl.), 45 (1991).
113. This work was supported by NSF grants DPP 8917076 (R.C.S., B.B.P., R.R.B., and S.M.) and DPP 9002872 (D.K.) and by National Aeronautics and Space Administration grant NAGW-290-10 (R.C.S.). We acknowledge the officers and crew of the R.V. *Polar Duke*, the Antarctic Support Associates, and other Icecolors '90 team members (K. Crocker, K. Hwang, S.-H. Kang, C. Johnson, R. Jovine, A. Marotti, M. Moline, A. Morell, N. Nelson, O. Schofield, and E. Stephens). A. Krueger provided the TOMS data, C. R. Booth provided data from the NSF Division of Polar Programs UV monitoring station, and A. Torres provided the Palmer balloon O_3 data. D. Clark helped design the LUVSS instrument, which was designed and built with NSF support (DPP88-17634, R.C.S.). This is Icecolors contribution 1.

Research Article

Structural Evidence for Induced Fit as a Mechanism for Antibody-Antigen Recognition

JAMES M. RINI, URSULA SCHULZE-GAHMEN, IAN A. WILSON*

The three-dimensional structure of a specific antibody (Fab 17/9) to a peptide immunogen from influenza virus hemagglutinin [HA1(75–110)] and two independent crystal complexes of this antibody with bound peptide (Tyr^{P100}-Leu^{P108}) have been determined by x-ray crystallographic techniques at 2.0 Å, 2.9 Å, and 3.1 Å resolution, respectively. The nonapeptide antigen assumes a type I β turn in the antibody combining site and interacts primarily with the Fab hypervariable loops L3, H2, and H3. Comparison of the bound and unbound Fab structures shows that a major rearrangement in the H3 loop accompanies antigen binding. This conformational change results in the creation of a binding pocket for the β turn of the peptide, allowing Tyr^{P105} to be accommodated. The conformation of the peptide bound to the antibody shows similarity to its cognate sequence in the HA1, suggesting a possible mechanism for the cross-reactivity of this Fab with monomeric hemagglutinin. The structures of the free and antigen bound antibodies demonstrate the flexibility of the antibody combining site and provide an example of induced fit as a mechanism for antibody-antigen recognition.

FUNDAMENTAL QUESTIONS CONCERNING THE STRUCTURAL basis of antibody-antigen recognition are still largely unanswered. Although hydrogen bonding, van der Waals contacts, salt bridges, and buried surface area are of critical significance (*1*), the contribution of conformational changes in the antibody or antigen upon complexation, which may range from small changes in side-chain torsional angles to domain rearrangements, has still to be assessed. The concept of inducible fit relaxes the requirement for an exact preexisting fit between antibody and antigen. Such inducibility occurs at the expense of specificity, and hence there should be limits on the magnitude of these changes (*2*). The extent to which either the antibody or antigen changes conformation has, in fact, been much discussed (*1–6*). Both the lock-and-key (*3*) and induced fit type mechanisms (*4–6*) have been used to describe antibody-antigen recognition.

The x-ray crystal structures of a few unliganded antibodies and antigens and their respective antibody-antigen complexes have been determined and indicate that small but significant changes in both the antigen and antibody can accompany complex formation (*1, 2, 4, 5*). Complexes of Fab fragments with lysozyme and with neuraminidase (*3, 7–9*) show differences in the antigen of up to 1 to 2 Å for backbone and 2 to 4 Å for side-chain atoms, whereas the Fab′ fragment of an antibody (B13I2) to a myohemerythrin peptide and its corresponding Fab′-peptide complex show similar changes in the antibody (*5*). In addition, small but significant differences in the relative orientation of the variable heavy and light chain (V_H and V_L) domains in the Fv fragment of an antibody to lysozyme (D1.3) have been observed between the bound and unbound forms (*4*). Domain changes of a larger magnitude have been observed for an antibody (BV04-1) to single-stranded DNA (*10*).

It is not yet clear how such changes manifest themselves in terms of the specificity and selectivity of antibody antigen interactions. The potential design of antibodies with tailored specificity and catalytic properties (*11*), however, requires that we understand in structural detail the role of conformational changes in antigen recognition.

We have now determined the three-dimensional structure of Fab 17/9 from a mouse immunoglobulin [IgG2a(κ)] to a peptide, corresponding to 36 amino acid residues [HA1(75 to 110) from the influenza virus hemagglutinin (HA), in both its unliganded form and in complex with its nonamer peptide antigen (Tyr^{P100}-Asp-Val-Pro-Asp-Tyr-Ala-Ser-Leu^{P108}-amide). This antibody, Fab 17/9, is one of a panel of 21 monoclonal antibodies whose peptide binding specificity has been well characterized (*12, 13*). The minimum epitope for Fab 17/9 corresponds to the six residues from Asp^{P101} to Ala^{P106}. The nonamer peptide binds to the antibody with 50 percent inhibition at 2×10^{-8} M as determined by competition enzyme-linked immunoabsorbent assay (ELISA). The cognate peptide sequence is on the monomer surface in the HA but is located in the trimer interface and, consequently, the antibody cannot bind to the trimeric HA at physiological pH (*12, 14*). At low pH, the HA

The authors are in the Department of Molecular Biology, The Scripps Research Institute, 10666 North Torrey Pines Road, La Jolla, CA 92037. The present address of J. M. Rini is Department of Molecular and Medical Genetics, University of Toronto, Toronto, Ontario, Canada M5S 1A8.

*To whom correspondence should be addressed.

trimeric heads undergo a partial dissociation and the trimeric HA can be cleaved by trypsin to yield monomeric "tops" [HA1(28–328)] (*15*) which are bound by Fab 17/9 with an affinity three to four orders of magnitude less than that of the nonamer peptide. Antibody binding to this biologically important, fusion-active form of the trimeric HA has also been demonstrated for other members of this panel of monoclonal antibodies (*16*).

It is of interest to determine how the dual recognition of the free peptide and the intact protein can be mediated by the same antibody. Since the epitope embedded in the intact protein is presented in an environment different from that of the peptide, either free in solution or coupled to a carrier protein, considerable accommodation in the antibody or the antigen (or both) might underlie the dual recognition capabilities of antibodies to peptides.

Crystallization and data collection. Unliganded Fab and monoclinic peptide complex were crystallized as described (*17*) with minor modification. The unliganded (native) Fab (10 mg/ml) was crystallized from 0.2 M imidazole-malate buffer (pH 5.6 to 6.5) containing 0.1 M NaCl; polyethylene glycol (PEG) 600 (30 to 39 percent) was used as precipitant. The crystals are in space group $P2_1$ with unit cell dimensions of a = 90.4 Å, b = 82.8 Å, c = 73.4 Å, β = 122.6°. The asymmetric unit contains two Fab molecules, resulting in a solvent content of 46 percent. A monoclinic ($P2_1$) Fab-peptide complex was grown from 20 mM ammonium acetate (pH 5.5) containing 50 mM $MnCl_2$ at a PEG 600 concentration of 2 to 4 percent. The nonamer peptide was added in five times molar excess compared to the amount of Fab (10 mg/ml) (*17*). The unit cell dimensions of the complex crystals are a = 63.5 Å, b = 73.4 Å, c = 62.7 Å, β = 117.1°, and a single Fab-peptide complex in the asymmetric unit gives a solvent content of 53 percent. A second Fab-peptide crystal form was grown by macroseeding from 1.7 M ammonium sulfate, 0.2 M imidazole citrate (pH 6.5), and 1.8 percent PEG 600 with Fab at 4 mg/ml and a five times molar excess of peptide. The initial crystals were obtained from the same buffer at 2.2 M ammonium sulfate concentration. This crystal form is triclinic, with space group $P1$ (a = 60.1 Å, b = 67.1 Å, c = 73.2 Å, α = 89.9°, β = 101.8°, γ = 96.5°) and two molecules in the cell giving a solvent content of 61 percent. Data from all crystals were collected on a Siemens multiwire area detector mounted on an Elliott GX-18 x-ray generator, equipped with a 100-μm focus and Franks focusing optics (*18*) and processed with the XENGEN software package (*19*). A 2.0 Å data set for the unliganded Fab was collected from eight crystals with a merging R value of 0.09 on intensities. The triclinic crystal grew as a twin composed of two identical lattices related by an approximate 180° rotation about the a^*-axis. Data were integrated from each of the two lattices independently with the use of the appropriate orientation matrices in XENGEN, and overlapping reflections were discarded. Data to 2.9 Å (87 percent complete) were collected from 18 crystals with a merging R value of 0.12. Since the monoclinic Fab-peptide crystals were very small (0.3 by 0.04 by 0.02 mm), data were collected at −150°C to minimize the effects of radiation decay. Techniques similar to those described by Hope (*20*) were used to flash cool the crystal on a thin glass paddle in the cold nitrogen stream of the Siemens LT2 after a brief washing in mother liquor containing 35 percent ethylene glycol. A complete data set to 3.1 Å was collected from a single crystal in 10 days with a merging R value of 0.10.

Structure determination. The variable and constant domain models from McPC603 (*21*) and HyHEL-5 (*8*), respectively, were used in the molecular replacement solution of the native Fab. Each molecule in the asymmetric unit was solved independently with the 8 to 4 Å data (23 Å Patterson cutoff radius) with the use of the Crowther fast rotation function and the Crowther and Blow translation function implemented in the MERLOT program package (*22*). Of the five Fab structures available, all gave good rotation solutions for the variable domains, but only HyHEL-5, which like Fab 17/9 is a mouse IgG(κ), gave interpretable results for the constant domain. Rigid body refinement (eight domains) was performed with CORELS (*23*) and MATREF (*24*) to give a model with an R value of 0.42 for the 10.0 to 4.0 Å data. The hypervariable loops and all other residues differing from the input model were then manually built into OMIT maps (*25*) with the use of FRODO (*26*). Model refinement with the high-temperature simulated annealing protocol from X-PLOR (*27*) against the 8.0 to 2.5 Å data resulted in an R value of 0.25 with an overall temperature factor of 11.6 $Å^2$. Subsequently, manual rebuilding from OMIT maps and two cycles of the temperature bath cooling protocol were performed to incorporate first the 2.3 Å data and then the 2.0 Å data. The model, which includes 160 water molecules, has an R value of 0.195 for the 6.0 to 2.0 Å data ($F > 2\sigma_F$), with restrained individual atomic temperature factors. The root-mean-square (rms) deviations from ideality on bond lengths and angles are 0.015 Å and 3.0°, respectively.

Both complexes were solved with the use of partially refined coordinates of the native Fab. For the triclinic crystal form, well-defined rotation solutions, related by an approximate twofold rotation axis, were found for each of the variable and constant domains of both molecules in the unit cell. The two independent Fab's were placed on a common origin by computing a set of cross vectors between the two molecules and were then refined as rigid bodies (eight domains) to an R value of 0.38 for the 8.0 to 3.5 Å data. Refinement with the simulated annealing protocol of X-PLOR resulted in an R value of 0.24 for the 8 to 3 Å data. The Fab model was further rebuilt and refined as described above. Although electron density for the bound peptide was present at this stage, both this density and that for the H3 loop were still quite weak and discontinuous. A second cycle of simulated annealing was performed, and the difference electron density for the peptide was then averaged over both molecules in the unit cell (*28*). The peptide was initially built into the averaged map, but in subsequent rebuilding and refinement steps both molecules were treated independently in unaveraged maps. The model has an R value of 0.20 for the 8.0 to 2.9 Å data with restrained individual temperature factors with rms deviations from ideality on bond lengths and angles of 0.016 Å and 3.7°, respectively.

The monoclinic crystal form was solved generally as described above. In this case, however, the translation problem was solved with the search based on the correlation between observed and calculated intensities implemented in X-PLOR. Each domain was solved independently on an 0.5 Å grid with the use of the 8.0 to 4.0 Å data. The relative y coordinate between the variable and constant domains was determined by a one-dimensional search of the constant domain at each of the four choices of relative origin by incorporating the scattering contribution for the variable domain. Simulated annealing with X-PLOR gave a model with an R value of 0.24. Electron density for the bound peptide was clear at this stage. The electron density for the protein interior was strong and well defined, but features on the surface of the protein seemed weaker and the noise level higher than that in our other Fab determinations. Since the data were collected at low temperature (−150°C), this may result from surface features with multiple conformations or ordered solvent structure that is not easily modeled at this resolution. The model has an R value of 0.22 for the 8.0 to 3.1 Å data with restrained atomic temperature factors and 22 well-ordered water molecules. The rms deviations from ideality on bond lengths and angles are 0.019 Å and 3.9°, respectively.

The solvent-accessible surface areas on the Fab and the peptide were calculated according to the program MS (*29*), with a 1.7 Å

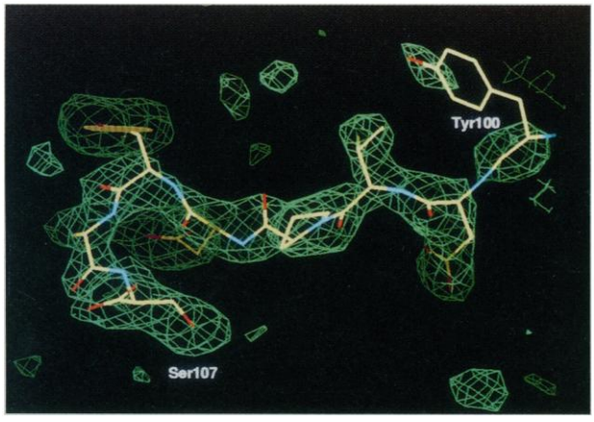

Fig. 1. Electron density for the bound peptide in an OMIT difference map (*25*) calculated for molecule 1 of the triclinic Fab peptide complex at 2.9 Å resolution. The map is contoured at 2.7 σ, and displayed with the program Tom FRODO on a Silicon Graphics personal IRIS work station. Density for residues 101 to 107 is continuous at 1.8 σ.

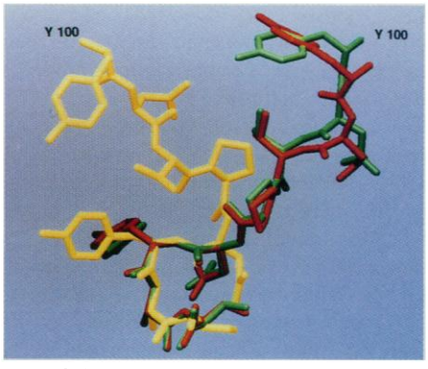

Fig. 2. Comparison of the structure of the peptide bound to the Fab and its cognate structure in the influenza virus hemagglutinin. The peptides were overlapped on the Cα atoms of the β-turn region (residues 104 to 107). The Fab-bound peptide conformations are shown in red (triclinic molecule 1) and green (monoclinic), and the corresponding HA peptide (*14*) is shown in yellow. Comparison of the Fab-bound peptides with the HA peptide shows similarity between the NH_2-terminal residues Tyr^{P100} to Pro^{P103} and between the COOH-terminal residues Asp^{P104} to Ser^{P107} (type I β turn). The major difference is in the ψ angle of Pro^{P103}.

probe radius and standard van der Waals radii (*30*). Hydrogen bonds and van der Waals contacts were assigned with the program CONTACSYM (*8, 31*). The Fab was numbered according to Kabat *et al.* (*32*) and the letters L, H, and P preceding the number designate light chain, heavy chain, and peptide, respectively.

Domain structure. Based on a pairwise comparison of the two native and three independent complex molecules, no significant change in the relative orientation of the V_L and V_H domains is seen on complex formation. The variable domains from all molecules were first superimposed on molecule 1 of the native structure with conserved residues from the V_H domain. The rotation and translation operation required to align the V_L domains were then calculated. While the values for the three Fab-peptide complexes were consistently larger than those for the two unliganded Fabs (4.1° and 0.43 Å, 4.2° and 0.86 Å, 3.4° and 0.86 Å compared to 2.9° and 0.29 Å), the differences did not exceed those found for a similar analysis with the constant domains (1.9° and 0.60 Å, 1.5° and 0.37 Å, and 1.7° and 0.54 Å compared to 0.7° and 0.01 Å). Thus, if domain rearrangements occur, they are of the order of a degree in rotation and a few tenths of an angstrom in translation. Calculation of the elbow angle that relates the pseudo-twofold rotation axes within the V_L and V_H and within the C_L and C_H1 domains gives values of 159° for the two unliganded Fab moieties, and 173°, 171°, and 175° for the two triclinic and monoclinic Fab-peptide complexes [calculated as in (*5*)]. Although these values might suggest a bound and unbound form of the Fab, the close agreement shown by the unbound forms can be explained by the pseudo-centered nature of the monoclinic crystal lattice, whereas similarity among the peptide bound forms likely reflects a common packing interaction along the 73 Å axis.

Peptide conformation. Comparison of the Fab-peptide complexes from the monoclinic and triclinic crystal forms shows that all three crystallographically independent complexes are similar. All show electron density for the first eight residues of the nonapeptide and, in addition, molecule 2 of the triclinic form shows density for Leu^{P108}. The NH_2-terminal residues (Tyr^{P100}-Asp-Val-Pro^{P103}) of the bound peptide are found in an extended conformation while the COOH-terminal residues (Asp^{P104}-Tyr-Ala-Ser^{P107}) adopt a type I β turn (Fig. 1). Comparison of the peptide conformation with that of the corresponding sequence in the HA shows structural similarity with the amino and carboxyl portions of the peptide when they are

Table 1. Hydrogen bonds and van der Waals contacts in the Fab 17/9 peptide complexes. Fab residues that undergo hydrogen bonding with peptide residues also contribute to van der Waals contacts. Residues with van der Waals contacts only are listed separately. Specific atoms listed with the peptide residues indicate those atoms that hydrogen bond with Fab residues. The Fab residues (atoms) listed are all the residues (atoms) making contacts with the peptide in the three complexes. Not all of the interactions are necessarily found in one single complex, and the number of contacts given is the range for the three complexes. There are 13 to 15 hydrogen bonds and 89 to 92 total contacts made in each of the Fab-peptide complexes. H2, H3, L1, and L3 refer to the heavy chain CDR's 2 and 3 and light chain CDR's 1 and 3, respectively.

Peptide	Atom	Fab 17/9 contact residues		Contacts (no.)
		Hydrogen bonds	Van der Waals contacts only	
Y^{P100}	Oη	N^{52a} Nδ2 (H2), N^{52a} Oδ1 (H2)	R^{97} (H3)	0–5
D^{P101}	Oδ2	S^{52} Oγ (H2), N^{52a} Oδ1 (H2), G^{53} N (H2)	Y^{56} (H2)	16–22
	Oδ1	G^{53} N (H2), G^{54} N (H2), G^{55} N (H2)		
V^{P102}	N	N^{52a} Oδ1 (H2)	Y^{56} (H2), R^{97} (H3)	3–9
	O	S^{52} Oγ (H2)		
P^{P103}			Y^{56} (H2), Y^{58} (H2)	8–13
D^{P104*}	Oδ1, Oδ2	R^{95*} guanidinium (H3)	T^{50} (H2), Y^{58} (H2)	5–10
Y^{P105}	Oη	D^{91} Oδ1 (L3), R^{95} Nη1 (H3)	Y^{32} (L1), E^{96} (H3), E^{100} (H3)	24–35
		R^{95} Nη2 (H3), N^{100a} N (H3),		
		G^{100b} N (H3)		
A^{P106}	O	N^{94} N (L3), N^{94} Oδ1 (L3)	D^{91} (L3), Y^{92} (L3)	8–9
			S^{93} (L3), L^{96} (L3), R^{95} (H3)	
S^{P107}	Oγ	Y^{58} Oη (H2)		4–6
L^{P108}			Y^{92} (L3)	0–5
				Total 89–92

*Residues forming salt bridges.

The pairwise contacts were generated in CONTACSYM (*8, 31*) with a cutoff of 3.4 Å for hydrogen bonds and salt bridges and up to 4.11 Å (depending on the atom types) for van der Waals contacts. Amino acid residues are listed with the one-letter code (*39*).

superimposed independently. The turn in the peptide resembles the type I turn for the same residues in the HA (Fig. 2). Likewise, residues 100 to 102 adopt a similar extended conformation in both the peptide and protein. With the exception of Pro^{P103}, the changes in ϕ and ψ values are small, indicating conformational similarity for each half of the peptide but difference in the overall shape of residues 100 to 107 in the peptide and protein antigen. Clearly, only a subset of the interactions seen in the Fab peptide complex are possible when the Fab binds the protein epitope. This fact coupled with the decreased accessibility of the protein epitope presumably accounts for the reduced affinity for HA "tops."

Antibody-antigen interaction. The peptide interacts primarily with the hypervariable loops or complementarity determining regions (CDR) L3, H2, and H3 (Fig. 3). On average, the peptides make 14, 45, and 29 pairwise contacts with each of these loops, respectively. There are no contacts with hypervariable loops L2 and H1 and only one or two contacts with L1. The number of hydrogen bonds and salt bridges between peptide and Fab ranges from 13 to 15 for the three crystallographically independent complexes and involve 11 Fab residues (Table 1). The total number of contacts between bound peptide and Fab ranges from 89 to 92, and involves 21 Fab residues (Table 1). As in other Fab complexes (*34*), the interactions with antigen are dominated by aromatic residues, small hydrophilic residues, and charged residues for salt-bridge formation. Except for Leu^{L96} there are no small aliphatic residues in contact with the peptide antigen.

The NH_2-terminus of the bound peptide (100 to 103) adopts an extended conformation in the Fab binding site and interacts primarily with residues of the H2 loop. The average temperature factors for these residues are higher than those for the COOH-terminal β turn, suggesting that they interact less tightly with the Fab. Tyr^{P100} is particularly disordered with little or no electron density for its side chain. Tyr^{P100} has no Fab contacts in the monoclinic crystal form but has three to five interactions and one crystal contact in the triclinic crystal form (Table 1).

In contrast, Asp^{P101}, a key residue of this peptide epitope, makes between 16 and 22 contacts with the Fab (Table 1). Despite its central role in binding, the electron density for its side chain in both crystal forms is weak, as is the density for its contact residues in the Fab molecule, making it difficult to accurately position its carboxyl group. However, it clearly interacts with the side chains of Ser^{H52} and Asn^{H52a} as well as the three glycine residues, Gly^{H53} to Gly^{H55}, which form the tip of the H2 loop. The peptide bond orientation between Gly^{H55} and Tyr^{H56} appears to be different in the two complex crystal forms, although the density in each is fairly weak, resulting in a different combination of hydrogen bonds between the Asp^{101} carboxyl group and the amide groups of Gly^{H53}-Gly^{H55}.

The amide nitrogen of Val^{P102} makes a hydrogen bond with the side chain of Asn^{H52a} of the Fab in all complexes and a hydrogen bond with the hydroxyl group of Ser^{H52} in the triclinic complex. There are no hydrogen bonds to the carbonyl oxygen of Pro^{P103} of the peptide. However, the proline ring does form van der Waals contacts with the side chains of Tyr^{H56} and Tyr^{H58}, which define one edge of the binding pocket.

Residues Asp^{P104}-Ser^{P107} adopt a type I β turn in the Fab binding site and primarily make contacts with residues of the H3 and L3 hypervariable loops. The β turn is more deeply buried in the Fab binding site than the NH_2-terminal region of the peptide. It is consequently more immobilized, as reflected by the average temperature factors and is probably responsible for the major portion of the stabilization energy. Asp^{P104} forms a buried salt bridge with Arg^{H95} of the H3 loop. This is the only interaction that involves charge neutralization in this complex. In addition, Arg^{H95} forms a stacking interaction with Tyr^{P105} which is further sandwiched by Glu^{H100}. The hydroxyl group of Tyr^{P105} is hydrogen bonded to one or more of Asp^{L91}, Arg^{H95}, Asn^{H100a}, and Gly^{H100b} in the different complexes. In total, Tyr^{P105} makes between 24 and 35 contacts with the Fab. The carbonyl oxygen of Ala^{P106} makes a very good hydrogen bond with the backbone amide group of Asn^{L94} in all three complexes.

The peptide surface areas buried on binding are 397, 419, and 448 $Å^2$ for the monoclinic and the two triclinic complexes respectively. In reference to the Fab' B13I2-peptide complex (*5*), Colman (*35*) pointed out that, since the peptide adopted a β turn in the Fab binding site, the surface area buried on binding may in fact be an underestimate. We have calculated that, in an extended β conformation, residues 100 to 107 would present an accessible surface area of 799 as compared to 740 $Å^2$ in the conformation found in the Fab-peptide complex. Since in this case (*36*), as with B13I2 (*37*), there is no evidence for secondary structure in solution for the peptide residues bound by the Fab, our estimates of surface area buried on binding may be underestimated by some 7 to 8 percent. Analysis by residue shows that approximately 110 $Å^2$ of the buried surface area on the peptide is contributed by Tyr^{P105}, between 50

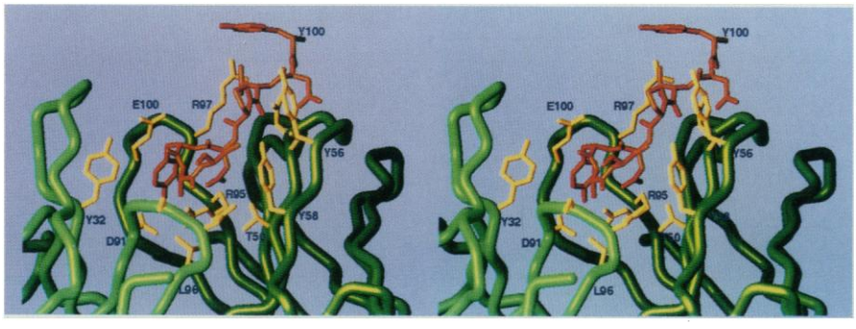

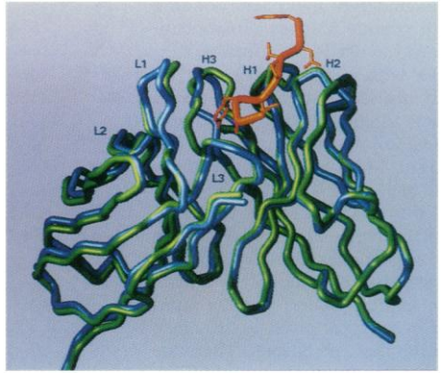

Fig. 3 (Left). Stereoview of the binding pocket of the Fab with residues contacting the bound peptide (red) highlighted in yellow. The Cα atom backbones of the V_H and V_L domains are shown in dark and light green, respectively. Molecule 1 of the triclinic crystal form is shown. Fab and peptide residues are numbered only where clarity permits. Tube models in Figs. 3, 4, and 6 were calculated with the program MCS (*33*). **Fig. 4 (Right).** Comparison of the Cα atom backbone of the Fv domain (V_H and V_L) of the liganded and unliganded Fab. Molecule 1 of the triclinic Fab-peptide complex (green) was superimposed on molecule 1 of the native Fab (blue), with the Cα atoms of residues 2 to 7, 16 to 24, 33 to 40, 66 to 72, and 89 to 95 from the V_H domain. In addition to the Cα atoms, side chains are shown for the bound peptide (red). The hypervariable loops of the light and heavy chain are marked L1-3 and H1-3, respectively. A major conformational change in the H3 loop is evident.

and 60 Å^2 by each of Asp^{P101}, Val^{P102}, Asp^{P104}, and Ala^{P106}, and from 25 to 30 Å^2 by Pro^{P103} and Ser^{P107}. The corresponding buried surface in the Fab for the three complexes ranges from 446 to 543 Å^2, of which about 6 percent is contributed by hypervariable loop L1, 20 percent by L3, 43 percent by H2, and 31 percent by H3. As in the B13I2 Fab′-peptide complex (*5*), about three-fourths of the contact surface is contributed by the heavy chain. Like other Fab-antigen complexes, there is close complementarity between the buried surfaces on the antigen and Fab. The fit is particularly good around Asp^{P101} and the β turn region of the peptide.

The Fab-peptide interactions seen in the x-ray structure agree well with the results of epitope mapping with a series of substitution analogs of a 13-residue peptide (HA1, 98 to 110). The reactivity of peptide analogs substituted with each of the 20 possible amino acids in position 101 to 106 was measured by inhibition ELISA (*38*), which showed that Asp^{P101} and Tyr^{P105} are the critical residues for binding with the affinity being on average 800 to 2000 times lower on substitution. Substitution of Asp^{P104}, which forms the salt bridge with Arg^{H95}, results in an average 400 times lower affinity. Since the main contribution to binding from Ala^{P106} involves a hydrogen bond to its carbonyl oxygen, it is not surprising that this side chain substitution results only in an average 35 times decrease in affinity. For Val^{P102} and Pro^{P103} the decrease in affinity is only 5 and 8 times, respectively, as would be expected from the limited interactions that they make with the Fab molecule.

The number of contacts between Fab 17/9 and its peptide antigen are comparable to those of other Fab-protein or Fab-peptide complexes (*1–5, 8, 9*). In the three lysozyme complexes (D1.3, HyHEL-5, and HyHEL-10) and the peptide complex (B13I2), the number of hydrogen bonds (10 to 15), salt bridges (0 to 3), and van der Waals contacts (65 to 111) are comparable with those that we found (13 to 15 hydrogen bonds; 1 salt bridge, and 74 to 81 van der Waals contacts). Moreover, as discussed by Stanfield *et al.* (*5*), the respective Fab and antigen-buried surface areas (540 Å and 460 Å^2) for the B13I2 Fab′-peptide complex are not much less than those found in the Fab-lysozyme complexes [for example, HyHEL-5 750 Å^2 and 750 Å^2], even though the number of antigen contact residues is much smaller for the peptide (7 for B13I2) than for the proteins (17 in HyHEL-5; 19 in HyHEL-10). This is also true for the 17/9 Fab-peptide complex where the corresponding values for the Fab and antigen buried surfaces are 476 and 420 Å^2 for molecule 1 of the triclinic form. Furthermore, the number of Fab residues contacting the antigen is similar for the protein (*1*) and peptide (*5*) complexes (14 to 21 compared to 18) despite the differences in the size of the ligand.

Table 2. The rms deviations between free and bound Fab for residues in the H3 loop. The V_H domain of the Fab's were superimposed onto the V_H domain of the native Fab 17/9 (mol 1), with the Cα atoms of residues 2 to 7, 16 to 24, 33 to 40, 66 to 72, and 89 to 95. The rms deviations were calculated between the native molecule 1 and the various complexes: the monoclonic ($P2_1$), the triclinic molecule 1 (*P1* mol 1), and the triclinic molecule 2 (*P1* mol 2). As a control the rms deviations between the two native molecules and between the various complexes were also calculated, which show rms deviations for the main chain and side chain of the H3 loop (95 to 102) of 0.2 and 0.4 Å (nat 1 and nat 2), 0.4 and 0.8 Å (*P1* mol 1 and *P1* mol 2), 0.8 and 1.3 Å (*P1* mol 1 and $P2_1$). Only the H3 loop shows a significantly and consistently higher rms deviation for the backbone between all the Fab-peptide complexes and the native molecule 1 than in between the various complex forms and between the two native molecules (on average 2.3 versus 0.5 Å).

Fab residue (H3)	Deviation (rms)					
	Main chain (Å)			Side chain (Å)		
	P1 mol 1	*P1* mol 2	$P2_1$	*P1* mol 1	*P1* mol 2	$P2_1$
R^{95}	0.5	0.7	0.6	1.0	0.9	1.2
E^{96}	1.2	1.0	1.1	1.6	1.2	1.0
R^{97}	3.2	3.1	2.5	5.4	5.4	4.9
Y^{98}	1.9	2.1	1.7	4.6	4.8	4.7
D^{99}	2.6	2.8	3.0	7.9	8.5	8.5
E^{100}	1.8	1.8	1.7	8.9	8.9	7.6
N^{100a}	3.7	3.8	3.9	7.7	7.6	7.8
G^{100b}	2.9	2.6	2.2			
F^{100c}	1.7	1.6	1.4	2.3	2.3	1.3
A^{101}	3.0	3.0	2.9	2.1	2.1	2.4
Y^{102}	2.0	2.0	1.6	0.9	0.9	0.9
R^{95}-Y^{102}	2.4	2.4	2.3	4.9	4.9	4.6

For both peptide antibodies (B13I2 and 17/9), the comparatively large contact area is achieved by embedding parts of the peptide into a deep groove and pocket on the Fab surface. Interestingly, the seven-residue epitope, EVVPHKK (*39*), of the bound peptide in the B13I2 complex and the corresponding peptide epitope, DVP-DYAS, in the 17/9 complex, is bound in the antibody binding site in a similar way. In each case, the first residue of the epitope (E or D) participates in peptide binding and forms hydrogen bonds with main-chain amides or serine hydroxyl within residues 52 to 55 of the H2 loop. The residues, VV or VP, make limited contacts with the Fab and can be replaced by other residues without substantially reducing the affinity (*38, 40*). Finally, the four COOH-terminal residues form β turns in both cases (VPHK type II and DYAS type

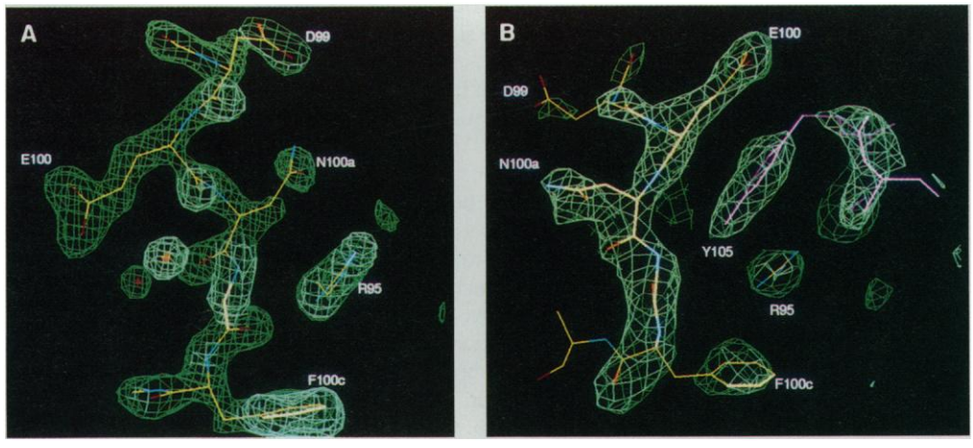

Fig. 5. Electron density in the antibody combining site for the H3 loop in the unliganded Fab and the Fab-peptide complex. Both molecules are shown in the same orientation. (**A**) OMIT difference electron density map at 2.0 Å resolution showing residues 95 and 99 to 100c of the H3 loop for molecule 1 of the native Fab. The density next to the carbonyl group of Asn^{100a} shows two ordered solvent molecules. (**B**) OMIT difference electron density map (2.9 Å resolution) for the same residues of molecule 1 in the triclinic Fab-peptide complex including residues 104 to 107 of the peptide. The peptide residues are shown in pink. In the native molecule, Asn^{H100a} is in the volume occupied by Tyr^{P105} of the peptide in the Fab-peptide complex. Conformational changes in the Fab in this region result in a pocket being formed to accomodate the key Tyr^{P105} side chain of the peptide antigen.

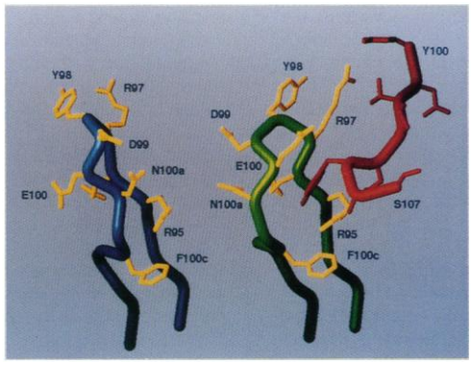

Fig. 6. Comparison of the conformation of the H3 loop in the unliganded Fab and the Fab-peptide complex. The Cα atom backbone of the H3 loop of the free Fab (blue) and the complex (green) are shown in the same orientation with their side chains in yellow. The Cα and side-chain atoms of the peptide are shown in red. Residues Asp^{H99}-Asn^{H100a}, in particular, have substantially different conformations in the free and bound forms.

I) and are tightly bound in a pocket formed mainly by residues from the H3 and L3 hypervariable loops. Although it is unlikely that all short peptides will assume β-turn conformations in antibody combining sites, the present Fab-peptide structures show that it is a good way to maximize the total buried surface on the peptide while maintaining a good fit to the pocket formed between the L3 and H3 loops.

Conformational changes. A comparison of the unbound and bound forms of Fab 17/9 shows that a major conformational change in the H3 loop is associated with peptide binding (Fig. 4 and Table 2). The hypervariable loops H1, H2, L2, and L3 retain similar conformations while the L1 loop shows more variability largely because of differences in packing among the three crystal forms (*41*). The rearrangement of the H3 loop would seem to be primarily a result of accommodating Tyr^{P105} of the peptide. Asn^{H100a} in the unliganded Fab, occupies the volume filled by Tyr^{P105} of the peptide in the complex (Fig. 5). Clearly, the Fab in the unliganded conformation would be unable to bind the peptide antigen.

In general terms, the change in conformation of the H3 loop can be described as a twisting of the two strands about the long axis of the loop (Fig. 6). As a result, three residues in particular are found to assume entirely different orientations in the bound and unbound forms. Asn^{H100a} rotates to the distal side of the H3 loop where it now points away from the binding site. Concomitantly, Asp^{H99} and Glu^{H100} flip from one side of the H3 loop to the other. The average shift in Cα position for the three complexes is 3.9, 2.0 and 4.6 Å for Asp^{H99}, Glu^{H100}, and Asn^{H100a}, respectively. The φ and ψ values for these residues change from 61° and 22°, −78° and 44°, 58° and −126° to −92° and −9°, 47° and 59°, and −143° and 72° on peptide binding (for molecule 1 of the native and triclinic complexes, respectively). Other H3 loop residues also show significant shifts in position (Table 2).

Analysis of the H3 loop conformation shows that it changes from an αα reverse turn to an αααα double turn on peptide binding, as defined by Wilmot *et al.* (*42*). Furthermore, Asn^{H100a}, which like Gly^{H100b} is found in the epsilon conformation in the native molecule, assumes a more favorable conformation between the αβ region of φ and ψ space in the complexes (*43*). As a result of these changes, the beta strands appear to open enough to accommodate the peptide, resulting in the net loss of two main-chain hydrogen bonds between the strands of the loop. In the native structure, five hydrogen bonds connect the main chain at residues 94 to 102, whereas in the complexes three different hydrogen bonds are made.

In the native structure, only four main-chain hydrogen bonds are made between the H3 loop and the rest of the Fab. Of these, only one is broken on peptide binding (Asp^{H99}-Trp^{L50}) to be replaced by an alternative hydrogen bond (Glu^{H100}-Trp^{L50}). In contrast, the side-chain hydrogen bonds differ considerably in the bound and unbound forms. Van der Waals interactions are also affected, most notably those involving Glu^{H100}, which in the native structure makes side-chain contacts with Tyr^{L49}. In the complex these contacts are replaced by the extensive stacking interaction of Glu^{H100} with Tyr^{P105} (average shift in Glu^{H100} Cδ is 9.1 Å). Remarkably, Tyr^{L49} now makes van der Waals contacts with Asn^{H100a}. The side chains of Arg^{H97} and Glu^{H100} interact with symmetry-related molecules in the triclinic crystal form. Since these interactions are not common to the monoclinic form, whose H3 loop is essentially identical in conformation, they must not make a significant contribution to the observed H3 loop conformation in the peptide complexes. In the native structure, the only crystal contacts involving the H3 loop are van der Waals interactions with the side chain of Tyr^{H98} at the tip of the H3 loop. Although this may affect the side chain rotamer somewhat, the overall loop conformation is dictated by the extensive hydrogen bond network within the H3 loop.

Induced fit. Wilson *et al.* (*44*) have analyzed the shape of the antigen binding site from a number of Fab complexes with antigens ranging from small haptens to proteins. Although the total surface areas buried by the various antigens is often similar, the surface

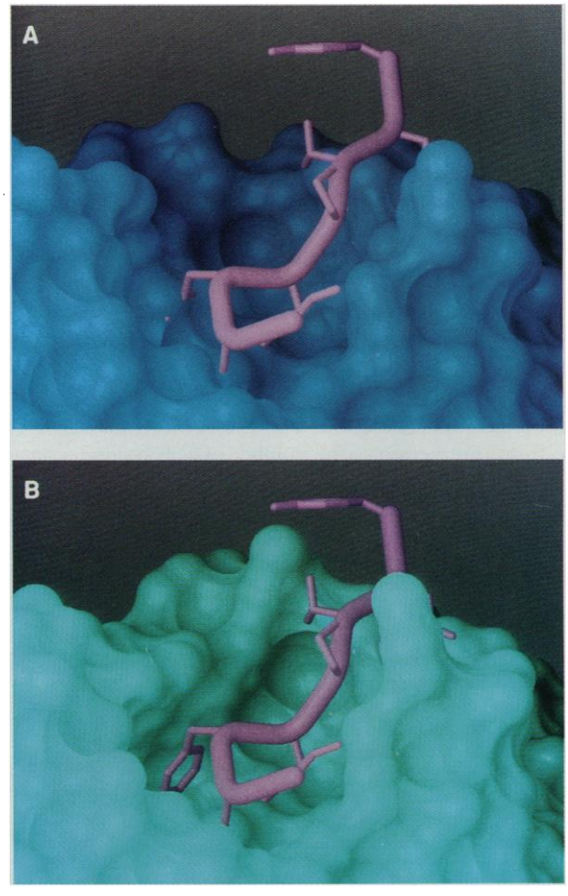

Fig. 7. Shape of the binding pockets of the unliganded and liganded Fab. Solvent accessible surface for the binding pocket of the unliganded Fab (blue) (**A**) and the Fab-peptide complex (green) (**B**) were calculated with the programs AMS (*29*) and MCS (*33*) with a 1.7 Å probe radius. For the native molecule in (A) the peptide (pink) was positioned as in the complex in order to illustrate the conformational changes that are made on peptide binding. A substantial difference in the shape of the combining site can be seen between the unliganded and peptide bound form of the Fab.

contours seen by the antigen differ. To assess the extent to which the H3 loop conformation affects the shape of the Fab 17/9 binding site, we calculated both the buried surface in the peptide complex and the corresponding surface for the native molecule (Fig. 7). The unliganded Fab appears as an open, basin-shaped pocket, whereas in the liganded Fab, a prominant groove connected to a deep pocket is formed to fit the peptide antigen. The most striking change in the shape of the binding site is the creation of a binding pocket for Tyr^{P105} and the formation of a very prominent channel to encompass the extended portion of the bound peptide. The difference in the two conformational forms of the Fab (liganded and unliganded) illustrates the induced fit of an antibody to an antigen.

The antibody-antigen and protease-inhibitor complexes determined up until now have been characterized by small conformational changes involving interacting surfaces that are not highly mobile (*45*). The rapidly growing data base of Fab structures lends some support to this view with the emergence of canonical hypervariable loop conformations (*46*). In the Fab 1719 structures presented, we find that the hypervariable loops are well defined and give no evidence for multiple conformations in either the complex structures or the high resolution native structure. There is, however, a large change in the H3 loop conformation between the unbound and bound Fab. Thus, a distinction between mobility and the ability to assume more than one conformation may have to be made. The native structure described above is incapable of binding peptide, and a new conformation that is intimately associated with the bound peptide is found in the complex. This does not necessarily suggest that the loop is highly mobile or adopts multiple conformations. The peptide bound conformation of the H3 loop may be energetically and kinetically accessible only in the presence of peptide. If so, this induced fit mechanism may be a means of selecting a productive binding mode without the entropic expense of immobilizing a flexible loop.

Because the monoclonal antibody Fab 17/9 was obtained from hyperimmunized mice and has therefore has undergone affinity maturation, the question arises whether the primary antibody used already an induced fit mechanism for peptide binding or whether the induced fit appeared during the maturation toward the high affinity antibody. The possibility of induced fit in the antibody binding pocket needs to be considered in the attempt to induce anti-idiotypic antibodies, which are thought to be "internal images" of external antigens (*47*). Anti-idiotypic antibodies of this type would have to be complementary to the induced "binding conformation" of the antibody.

The conformational change described above is in contrast with what has been observed, with other antibody-antigen complexes. In these other cases, either small localized shifts in a few residues (*1*), small shifts in domain associations (*4, 10*), or the segmental motions of a portion of a hypervariable loop (*5*) have been observed. In Fab 17/9 we see two apparently well-defined conformations for the H3 loop, and these differ in the architecture of the whole loop. Taken together, however, it seems likely that inducibility of fit spans a considerable range of movements in the formation of antibody-antigen complexes. Analysis of the unliganded structure alone may not be sufficient to define the shape of the antibody combining site with which the antigen interacts.

REFERENCES AND NOTES

1. D. R. Davies, E. A. Padlan, S. Sheriff, *Annu. Rev. Biochem.* **59**, 439 (1990).
2. P. M. Colman, *Adv. Immunol.* **43**, 99 (1988).
3. A. G. Amit, R. A. Mariuzza, S. E. V. Phillips, R. J. Poljak, *Science* **233**, 747 (1986).
4. T. N. Bhat, G. A. Bentley, T. O. Fischmann, G. Boulot, R. J. Poljak, *Nature* **347**, 483 (1990).
5. R. L. Stanfield, T. M. Fieser, R. A. Lerner, I. A. Wilson, *Science* **248**, 712 (1990).
6. E. D. Getzoff *et al.*, *ibid.* **235**, 1191 (1987); P. M. Colman *et al.*, *Nature* **326**, 358 (1987).
7. P. M. Colman *et al.*, *Philos. Trans. R. Soc. London, Ser. B* **323**, 511 (1989).
8. S. Sheriff *et al.*, *Proc. Natl. Acad. Sci. U.S.A.* **84**, 8075 (1987).
9. E. A. Padlan *et al.*, *ibid.* **86**, 5938 (1989).
10. J. N. Herron *et al.*, *Proteins Struct. Funct. Genet.* **11**, 159 (1991).
11. P. G. Schultz, R. A. Lerner, S. J. Benkovic, *Chem. Eng. News* **68**, 26 (1990); R. A. Lerner and S. J. Benkovic, *BioEssays* **9**, 107 (1988); J. S. Huston *et al.*, *Proc. Natl. Acad. Sci. U.S.A.* **85**, 5879 (1988).
12. I. A. Wilson *et al.*, *Cell* **37**, 767 (1984).
13. R. A. Houghten, S. R. Hoffman, H. L. Niman, in *Vaccines 86*, F. Brown, R. M. Chanock, R. A. Lerner Eds. (Cold Spring Harbor Laboratory, Cold Spring Harbor, NY, 1986), pp. 21–25.
14. I. A. Wilson, J. J. Skehel, D. C. Wiley, *Nature* **289**, 366 (1981).
15. J. J. Skehel *et al.*, *Proc. Natl. Acad. Sci. U.S.A.* **79**, 968 (1982).
16. J. M. White and I. A. Wilson, *J. Cell Biol.* **105**, 2887 (1987).
17. U. Schulze-Gahmen *et al.*, *J. Biol. Chem.* **263**, 17100 (1988).
18. S. C. Harrison, *J. Appl. Crystallogr.* **1**, 84 (1968).
19. A. J. Howard *et al.*, *ibid.* **20**, 383 (1987).
20. H. Hope, *Acta Crystallogr.* **B44**, 22 (1988); H. Hope *et al.*, *ibid.* **B45**, 190 (1989).
21. Y. Satow, G. H. Cohen, E. A. Padlan, D. R. Davies, *J. Mol. Biol.* **190**, 593 (1986).
22. P. M. D. Fitzgerald, *J. Appl. Crystallogr.* **21**, 273 (1988).
23. J. L. Sussman, S. R. Holbrook, G. M. Church, S.-H. Kim, *Acta Crystallogr.* **A33**, 800 (1977).
24. T. O. Yeates and D. C. Rees, *J. Appl. Crystallogr.* **21**, 925 (1988).
25. T. N. Bhat and G. H. Cohen, *ibid.* **17**, 244 (1984). For OMIT map calculations, 5 to 10 percent of the residues in the asymmetric unit were deleted from the model. The OMIT model was subjected to 40 cycles of positional refinement with XPLOR before the map calculation, to reduce model bias.
26. A. T. Jones, *J. Appl. Crystallogr.* **11**, 268 (1978).
27. A. T. Brünger, J. Kuriyan, M. Karplus, *Science* **235**, 458 (1987).
28. Programs written by D. J. Filman at the Scripps Research Institute.
29. M. L. Connolly, *J. Appl. Crystallogr.* **16**, 548 (1983).
30. D. A. Case and M. Karplus, *J. Mol. Biol.* **132**, 343 (1979).
31. S. Sheriff, W. A. Hendrickson, Y. L. Smith, *ibid.* **197**, 273 (1987). CONTACTSYM was written by S. Sheriff.
32. E. A. Kabat, T. T. Wu, M. Reid-Miller, H. M. Perry, K. S. Gottesman, *Sequences of Proteins of Immunological Interest* (National Institutes of Health, Bethesda, MD, ed. 4, 1987).
33. M. L. Connolly, *J. Mol. Graph.* **3**, 19 (1985).
34. E. A. Padlan, *Proteins: Structure, Function, Genet.* **7**, 112 (1990); I. S. Mian, A. R. Bradwell, A. J. Olson, *J. Mol. Biol.* **217**, 133 (1991).
35. P. M. Colman, *Current Opinion Struct. Biol.* **1**, 232 (1991).
36. H. J. Dyson *et al.*, *Nature* **318**, 480 (1985); H. J. Dyson, personal communication.
37. H. J. Dyson *et al.*, *J. Mol. Biol.* **201**, 201 (1988).
38. C. Pinilla, J. R. Appel, S. E. Mac Pherson, R. A. Houghten, in *Peptides, Proceedings of the Twelfth Peptide Symposium*, J. Smith, Ed. (Escom, Leiden, 1991), pp. 538–539.
39. Abbreviations for the amino acid residues are: A, Ala; C, Cys; D, Asp; E, Glu; F, Phe; G, Gly; H, His; I, Ile; K, Lys; L, Leu; M, Met; N, Asn; P, Pro; Q, Gln; R, Arg; S, Ser; T, Thr; V, Val; W, Trp; Y, Tyr.
40. H. M. Geysen, unpublished data.
41. Variation in the L1 loop conformation has also been seen in Fab' B13I2 (7).
42. C. M. Wilmot and J. M. Thornton, *Protein Eng.* **3**, 479 (1990). An αα reverse turn is defined where the distance between the Cα of residue i and the Cα of $i + 3$ is less than 7 Å apart and the $i + 1$ and $i + 2$ residues are both in an alpha conformation but are not part of a helix. An αααα double turn consists of two consecutive αα reverse turns where the second αα turn begins at residue $i + 1$ of the first αα turn.
43. A search of the Brookhaven data bank showed that, although relatively rare, two consecutive epsilon residues have been found in β hairpins, helix-helix connections and β-strand and helix loops.
44. I. A. Wilson *et al.*, in *Catalytic Antibodies, Ciba Foundation Symp.* **159** (Wiley, Chichester, 1991), pp. 13–39.
45. J. Janin and C. Chothia, *J. Biol. Chem.* **265**, 16027 (1990).
46. C. Chothia and A. M. Lesk, *J. Mol. Biol.* **196**, 901 (1987); ———, A. Tramontano, *Nature* **342**, 877 (1989).
47. N. K. Jerne, J. Roland, P.-A. Cazenave, *EMBO J.* **1**, 243 (1982); H. Köhler *et al.*, *Method Enzymol.* **178**, 3 (1989).

48. We thank R. Lerner for initiating the project on antibodies to peptides and for support, advice, and enthusiasm; H. Niman for the initial clones of Fab 17/9; G. Fieser for technical assistance; D. Filman for help with the map averaging procedure; C. Chothia, J. Thornton, S. Sheriff, and C. Wilmot for discussions; and M. Geysen for unpublished binding data. Supported by NIH grant AI-23498 (I.A.W.), by MRC (Canada) and Centennial Fellowships (Canada) (J.M.R.), and by a Deutsche Forschungsgesellschaft Fellowship (U.S.-G.). This is manuscript 6997MB from the Scripps Research Institute. Coordinates will be deposited in the Brookhaven Protein Data Bank.

3 September 1991; accepted 17 January 1992